Relativistic calculation of nondipole effects in high-order harmonic generation

I. A. Ivanov [1,*] and Kyung Taec Kim[1,2,†]

[1]*Center for Relativistic Laser Science, Institute for Basic Science (IBS), Gwangju 61005, Republic of Korea*

[2]*Department of Physics and Photon Science, GIST, Gwangju 61005, Republic of Korea*

(Received 31 July 2023; accepted 23 October 2023; published 8 November 2023)

We present results of relativistic calculations of even-order harmonic generation from various atomic targets. The even-order harmonics appear due to the relativistic nondipole effects. We take these relativistic effects into account by using an approach based on the solution of the time-dependent Dirac equation. The spectra of the nondipole even harmonics look qualitatively similar to the spectra of the dipole harmonics obeying the same classical cutoff rule. The temporal dynamics of the formation of the nondipole harmonics is, however, distinctly different from the process of dipole harmonics formation. Even-order harmonics emission is strongly suppressed at the beginning of the laser pulse, and the emission times of the nondipole harmonics are shifted with respect to the bursts of the dipole emission. These features are partly explained by a simple modification of the classical three-step model which takes into account selection rules governing the emission of harmonic photons.

DOI: 10.1103/PhysRevA.108.052808

I. INTRODUCTION

One can expect relativistic effects to play an important role in the dynamics of the processes of atomic or molecular interactions with strong laser pulses for laser intensities over 10^{18} W/cm^2 [1], when, with increasing ponderomotive energy, electron velocity can approach the speed of light in the vacuum. It has been realized since the pioneering paper by Reiss [2], however, that relativistic effects may reveal themselves even for moderately intense (10^{13}–10^{14} W/cm^2) low-frequency infrared (IR) laser fields. For instance, even for the IR laser fields of intensity of the order of 10^{13} W/cm^2, the relativistic effects are visible in the photoelectron spectra [3–9] in the tunneling regime of ionization, characterized by the values $\gamma \lesssim 1$, where $\gamma = \omega\sqrt{2|I_p|}/E_0$ is the Keldysh parameter [10], and ω, E_0, and I_p are the field frequency, field strength, and ionization potential of the target system expressed in atomic units. These relativistic nondipole effects are due to the influence of the magnetic field component of the laser pulse which induces a non-negligible momentum transfer to the photoelectrons [3,11]. Alternatively, if we prefer the photon picture of light, one might say that an IR photon carries small momentum, but a large number of the photons participating in the process of the tunneling ionization [12] deliver non-negligible momentum to the ionized electron [13,14].

The momentum delivered by the photons to the photoelectron was measured experimentally under the typical parameters of the tunneling ionization regime [11]. This momentum manifests itself, on average, as a shift of the photoelectron momentum distributions (PMDs) in the pulse propagation direction. A more detailed picture, which emerges as a result of the complex interplay of the magnetic and Coulomb forces, includes the so-called direct electrons which never recollide with the parent ion and are driven in the direction of the laser photon momentum, and the slow electrons which experience recollisions and may acquire momentum opposite to the photon momentum [5].

Theoretical study of these effects clearly necessitates methods which go beyond the commonly used nonrelativistic dipole approximation. A number of theoretical procedures allowing to consider relativistic nondipole effects have been described in the literature, including the relativistic strong-field approximation [8,9,15,16], time-dependent Schrödinger equation (TDSE) with nondipole corrections [6,13,14,17], an approach based on the nondipole strong-field-approximation Hamiltonian [18], and the time-dependent Dirac equation (TDDE) [19–22].

The nondipole effects manifest themselves as well in other processes occurring when atoms or molecules interact with laser fields. The process that interests us in the present work is the process of the high-order harmonic generation (HHG). The nondipole effects are known to produce several modifications in the HHG spectra. It was found [23] that the nondipole interactions lead to decrease of harmonic intensity and shift of odd-order harmonics in the spectra. A detailed investigation of the effect of the pulse magnetic field on harmonic spectra was reported in Refs. [24–26]. It was found [24] that the nondipole magnetic field effects result in the emission of photons polarized along the propagation direction which, for the laser pulse wavelength of 800 nm and intensity of the order of 5×10^{15} W/cm^2, is several orders of magnitude weaker than the photon emission polarized parallel to the driving pulse polarization direction. For stronger pulses with intensities of the order of 10^{17} W/cm^2, the magnetic field effects start playing a crucial role [26]. Electron drift in the laser propagation direction due to the magnetic-field component of the laser pulse prevents recollisions and hence, as one could expect on

*igorivanov@ibs.re.kr

†kyungtaec@gist.ac.kr

the basis of the picture provided by the celebrated three-step model of HHG [27,28], leads to the decrease of the harmonic emission.

Perhaps one of the most striking manifestations of the nondipole effects is the appearance of even-order harmonics in the HHG spectra [29–31], presenting an example of a relatively small perturbation producing not only relatively minor quantitative modifications of the spectra, but introducing a qualitative change: harmonics with frequencies forbidden in the dipole approximation. The appearance of the even-order harmonics can be understood as a result of the breakup of the well-known symmetry which the electron trajectories responsible for the emission of the harmonic photons exhibit in the dipole approximation [27]. Magnetic field effects break this symmetry, and thus make possible the generation of even-order harmonics. These harmonics were studied theoretically in Ref. [30], using perturbative treatment of the nondipole effects.

In the present paper we report a systematic theoretical study of the nondipole effects, in particular generation of the even-order harmonics, from various atomic targets. We use the TDDE as our main calculational tool, based on the previously developed procedure for the numerical solution of the time-dependent Dirac equation [21,22]. The approach based on the TDDE provides a complete nonperturbative description of the nondipole, as well as other relativistic effects.

Atomic units with $\hbar = 1$, $e = 1$, $m = 1$, and $c \approx 137.036$ (here e and m are charge and mass of the electron, c the speed of light) are used throughout the paper.

II. THEORY

A. Numerical solution to the time-dependent Dirac equation

We solve the TDDE,

$$i\frac{\partial \Psi(r,t)}{\partial t} = \hat{H}\Psi(r,t), \tag{1}$$

following the procedure we described in Refs. [21,22], which we briefly recapitulate below for the reader's convenience. In Eq. (1) $\Psi(r,t)$ is a four-component bispinor and the Hamiltonian operator has the form

$$\hat{H} = \hat{H}_{\rm atom} + \hat{H}_{\rm int}, \tag{2}$$

with

$$\hat{H}_{\rm atom} = c\boldsymbol{\alpha}\cdot\hat{\boldsymbol{p}} + c^2(\beta - I) + I\,V(r) \tag{3}$$

and

$$\hat{H}_{\rm int} = c\boldsymbol{\alpha}\cdot\hat{\boldsymbol{A}}. \tag{4}$$

In Eq. (3), $\boldsymbol{\alpha} = \left(\begin{smallmatrix}\mathbf{0} & \sigma\\ \sigma & \mathbf{0}\end{smallmatrix}\right)$, $\beta = \left(\begin{smallmatrix}I & \mathbf{0}\\ \mathbf{0} & -I\end{smallmatrix}\right)$, $I = \left(\begin{smallmatrix}I & \mathbf{0}\\ \mathbf{0} & I\end{smallmatrix}\right)$, $\boldsymbol{\sigma}$ are Pauli matrices, $\mathbf{0}$ and $\boldsymbol{I}$ are 2×2 null and identity matrices, $V(r)$ is the atomic potential, and $c = 137.036$ the speed of light. We subtracted from the field-free atomic Hamiltonian (3) the constant term Ic^2 corresponding to the rest mass energy of the electron.

We use a laser pulse linearly polarized in z and propagating in the x direction. The vector potential of the pulse is defined in terms of the pulse electric field:

$$\boldsymbol{A}(x,t) = -\hat{\boldsymbol{e}}_z\int_0^u E(\tau)\,d\tau, \tag{5}$$

where $u = t - x/c$. At any given point in space the pulse has a finite duration T_1 so that $E(\tau)$ in Eq. (5) is nonzero only for $0 < \tau < T_1$. As targets, we will consider below a model atom with a short-range (SR) Yukawa-type potential $V(r) = -1.903e^{-r}/r$, hydrogen atom, and helium atom described by means of an effective potential [32]. The target atom is initially in the ground s state $|\phi_0\rangle$ with an ionization potential (IP) of 0.5 a.u. for the hydrogen and Yukawa atoms and IP of 0.902 a.u. for the He atom.

The solution to Eq. (1) is expanded as a series in the basis bispinors:

$$\Psi(\mathbf{r},t) = \sum_{\substack{j\\ l=j\pm 1/2}}\sum_{M=-j}^{j}\Psi_{jlM}(\boldsymbol{r},t), \tag{6}$$

where

$$\Psi_{jlM}(\boldsymbol{r},t) = \begin{pmatrix} g_{jlM}(r,t)\Omega_{jlM}(\boldsymbol{n})\\ f_{jlM}(r,t)\Omega_{jl'M}(\boldsymbol{n})\end{pmatrix}, \tag{7}$$

and the two-component spherical spinors are defined as $\Omega_{jlM}(\boldsymbol{n}) = \left(\begin{smallmatrix} C^{jM}_{l\,M-\frac{1}{2}\,\frac{1}{2}\,\frac{1}{2}}Y_{l,M-\frac{1}{2}}(\boldsymbol{n})\\ C^{jM}_{l\,M+\frac{1}{2}\,\frac{1}{2}\,-\frac{1}{2}}Y_{l,M+\frac{1}{2}}(\boldsymbol{n})\end{smallmatrix}\right)$ (here $C^{jM}_{lm\frac{1}{2}\mu}$ are the Clebsch-Gordan coefficients, $Y_{lm}(\boldsymbol{n})$ spherical harmonics, and $\boldsymbol{n} = \boldsymbol{r}/r$). Parameters l and l' in Eq. (6) must satisfy the relation $l + l' = 2j$.

To take into account the nondipole effects due to the spatial dependence of the laser fields, vector potential (5) is expanded in a series of spherical harmonics at every time step of the integration procedure. Substituting expansion (6) and the expansion for the vector potential in the TDDE, Eq. (1), and using well-known properties of spherical spinors [33,34], one obtains a system of coupled differential equations for the radial functions $g_{jlM}(r,t)$ and $f_{jlM}(r,t)$ in Eq. (7). This system has been solved using a relativistic generalization of the well-known matrix iteration method (MIM) [35], which we described in detail in Ref. [21].

Appropriate choice of the propagation technique is essential, as the Dirac equation, as it is well known, possesses some properties which are absent in the case of the nonrelativistic wave equation. These properties are due to the presence of the continuum of the negative-energy states in the Dirac Hamiltonian which makes the Dirac Hamiltonian unbounded from below. One problem which this fact entails is the well-known problem of the collapse to the negative-energy continuum [36], which may manifest itself when basis set methods are used to construct approximations to the bound states of the Dirac Hamiltonian [36]. We avoid this problem, since we do not rely on the basis set methods. The initial state of the system is prepared in our calculation by solving numerically the eigenvalue equation for the field-free Dirac Hamiltonian employing the shooting method. A related problem is the so-called *Zitterbewegung* problem [37]. The presence of a superposition of the states with positive and negative energies implies that a solution to the TDDE should exhibit very fast oscillations with characteristic frequencies of the order of c^2.

Such oscillations are indeed present and we can reproduce them in the framework of our numerical procedure by using a sufficiently small integration time step Δ [21]. We had to use the time step Δ of the order of 10^{-6} a.u. in Ref. [21] to reproduce these oscillations. Use of such small values for Δ, if it were imperative, would make any practical calculations impossible, of course. Fortunately, one can bypass this problem by using an appropriate time-propagation technique. We discussed this issue in greater detail in Refs. [21,38]. For the reader's convenience we present a core of the argument below. From the purely numerical point of view, the presence of the fast oscillating terms in a system of ordinary differential equations (ODEs) gives us an example of a numerically stiff system of ODEs, i.e., a system in which vastly different timescales are present. To solve such a system of ODEs we must use a stable integration method [39], which ensures that while the numerical solution does not reproduce very fast oscillations, it describes accurately the overall behavior of the true solution. The integration procedure that we use provides such a stability. We can illustrate this point using a simple example of a stiff system of two ODEs:

$$i\dot{\boldsymbol{y}} = \boldsymbol{A}\cdot\boldsymbol{y}, \tag{8}$$

with Hermitian matrix $\boldsymbol{A} = \mathrm{diag}(\lambda_1(t), \lambda_2(t))$. To mimic the problem at hand let us assume that λ_1 is of order 1, while λ_2 has a large negative value on the interval of time that we consider. The short-time propagator in the MIM is a unitary Crank-Nicolson (CN) propagator [40], which relates solution vectors $\boldsymbol{y}_{n+1} = \boldsymbol{y}(t_{n+1})$ and $\boldsymbol{y}_n = \boldsymbol{y}(t_n)$ at times t_n and $t_{n+1} = t_n + \Delta$ as follows:

$$\boldsymbol{y}_{n+1} = \frac{1 - \frac{i\Delta}{2}\boldsymbol{A}(t_{n+1/2})}{1 + \frac{i\Delta}{2}\boldsymbol{A}(t_{n+1/2})}\boldsymbol{y}_n, \tag{9}$$

where $t_{n+1/2} = t_n + \Delta/2$. One can see from Eq. (9) that if at the nth step of the propagation the second component of the vector $\boldsymbol{y}$ acquires a numerical error $\delta y_n^{(2)}$, the unitarity of the CN propagation matrix in Eq. (9) makes this error remain bounded for $m > n$.

Spatial variables in the coupled differential equations for the radial functions $g_{jlM}(r,t)$ and $f_{jlM}(r,t)$ were discretized on a grid with the step size $\delta r = 0.05$ a.u., the radial variable was restricted to an interval $(0, R_{\max})$, with $R_{\max} = 400$ a.u., and angular momenta j up to 70 were included in expansion (6) in the calculations below. The propagation time step Δ was 0.05 a.u. Before proceeding to the description of the results of this calculation, it is instructive, however, to discuss an alternative treatment of the nondipole effects based on the leading-order perturbation theory (LOPT) expansion, as it provides a more transparent physical picture of the nondipole effects than the complete Dirac equation. The LOPT calculation described below was also used as an accuracy test for our solution to the TDDE.

B. LOPT treatment of the nondipole effects

We are interested in a LOPT solution to the TDDE considering the nondipole effects as relativistic corrections.

The leading-order relativistic corrections describing the nondipole effects in atom-field interaction can be obtained by expanding the minimal coupling atom-field interaction Hamiltonian [5,41,42] in the velocity gauge,

$$\hat{H}_{\mathrm{int}}^{\mathrm{min}}(t) = \hat{\boldsymbol{p}}\cdot\boldsymbol{A}(\boldsymbol{r},t) + \frac{\hat{\boldsymbol{A}}^2(\boldsymbol{r},t)}{2}, \tag{10}$$

in powers of c^{-1} [6]:

$$\hat{H}_{\mathrm{min}}(t) = \hat{p}_z A(t) + \frac{\hat{v}_z x E(t)}{c} + \frac{A^2(t)}{2} + O(c^{-2}), \tag{11}$$

where $E(t) = -\frac{\partial A(t)}{\partial t}$ is the electric field of the pulse, and the velocity operator $\hat{\boldsymbol{v}} = \hat{\boldsymbol{p}} + \boldsymbol{A}(t)$ has been introduced. The last term on the right-hand side (rhs) of Eq. (11) is a function of time only and can be removed by a unitary transformation of the wave function.

Including spin effects in the interaction Hamiltonian is not necessary, if we are interested in the effects of the leading order in powers of c^{-1} [5,23]. The fact that the spin degrees of freedom can be neglected in the leading order of the c^{-1} expansion can be understood using the semiclassical picture of the spin effects, in which additional force due to the presence of the spin degrees of freedom, acting on the electron, is $\boldsymbol{F} = -\boldsymbol{\nabla}U_m$, where $U_m = -\boldsymbol{\mu}\cdot\boldsymbol{H}$, the energy of the spin–magnetic field interaction. Here $\boldsymbol{H}$ is the magnetic field and $\boldsymbol{\mu}$ is the electron's magnetic moment related to the expectation value of the electron's spin, $\boldsymbol{\mu} = -2\boldsymbol{S}/c$. The spatial gradient of $\boldsymbol{H}$ introduces an additional factor of c^{-1}, making contribution of the force $\boldsymbol{F}$ an effect of higher order in c^{-1}. As for the relativistic corrections to the field-free atomic Hamiltonian, the so-called Breit-Pauli Hamiltonian [42], it adds terms of the order of c^{-2} to the nonrelativistic atomic Hamiltonian. We do not have, therefore, to include these corrections in the LOPT treatment. To the leading order in powers of the c^{-1} expansion, the dynamics of the system can thus be described by the TDSE:

$$i\frac{\partial\Psi(\boldsymbol{r},t)}{\partial t} = (\hat{H}_{\mathrm{atom}} + \hat{H}_{\mathrm{d}}(t) + \hat{H}_{\mathrm{nd}}(t))\Psi(\boldsymbol{r},t), \tag{12}$$

where

$$\hat{H}_{\mathrm{atom}} = \frac{\hat{\boldsymbol{p}}^2}{2} + V(r) \tag{13}$$

is the atomic field-free Hamiltonian,

$$\hat{H}_{\mathrm{d}}(t) = \hat{p}_z A(t) \tag{14}$$

is the dipole part of the atom-field interaction, and

$$\hat{H}_{\mathrm{nd}}(t) = \frac{\hat{v}_z x E(t)}{c} \tag{15}$$

is the nondipole part of the atom-field interaction containing the effects of the order of c^{-1}.

It is easy to check that the LOPT solution to Eq. (12), with the nondipole term (15) considered as a perturbation, can be written as

$$\Psi^{\mathrm{LOPT}}(\boldsymbol{r},t) = \Psi_{\mathrm{d}}(\boldsymbol{r},t) + \Psi_{\mathrm{nd}}^{(1)}(\boldsymbol{r},t), \tag{16}$$

where the LOPT nondipole correction is given by the expression

$$\Psi_{\mathrm{nd}}^{(1)}(\boldsymbol{r},t) = -i\int_0^t \hat{U}_{\mathrm{d}}(t,\tau)\hat{H}_{\mathrm{nd}}(\tau)\Psi_{\mathrm{d}}(\boldsymbol{r},\tau)\,d\tau. \tag{17}$$

As can be seen from Eq. (15) for the operator $\hat{H}_{\rm nd}$ this correction is of the order of c^{-1}. In Eqs. (16) and (17) $\Psi_{\rm d}(\boldsymbol{r},t)$ is the zero-order solution to the nonrelativistic TDSE taking into account only the dipole part of the atom-field interaction, and $\hat{U}_{\rm d}(t,\tau)$ is the evolution operator describing evolution of the system driven by the nonrelativistic dipole Hamiltonian. $\hat{U}_{\rm d}(t,\tau)$ satisfies the operator equation,

$$i\frac{\partial \hat{U}_{\rm d}(t,\tau)}{\partial t} = (\hat{H}_{\rm atom} + \hat{H}_{\rm d}(t))\hat{U}_{\rm d}(t,\tau), \tag{18}$$

and the initial condition $\hat{U}_{\rm d}(\tau,\tau) = \hat{I}$. In practice, we need not solve the operator equation (18). All we have to do to compute the expression under the integral on the rhs of Eq. (16) for given τ and t is to propagate first the initial-state wave function on the interval $(0,\tau)$ using the nonrelativistic TDSE with Hamiltonian (14), obtaining thus a state vector $\Psi_{\rm d}(\tau)$. We act then on this vector with the operator $\hat{H}_{\rm nd}(\tau)$ and propagate it further in time until the moment t. The nonrelativistic TDSE was solved using the well-tested numerical procedure described in Ref. [43].

C. Calculation of electron velocity and HHG spectra

Once the solution to the TDDE (1) is obtained, expectation values of the electron velocity can be obtained as [44]

$$\boldsymbol{v}(t) = c\langle\Psi(t)|\boldsymbol{\alpha}|\Psi(t)\rangle. \tag{19}$$

Harmonic spectra can then be calculated using the usual semiclassical approach, in which the spectral intensity of the harmonic emission can be expressed in terms of the Fourier transform of the electron's velocity:

$$S_a(\Omega) \propto \left|\int_0^{T_1} v_a(t)W(t)e^{i\Omega t}\,dt\right|^2, \tag{20}$$

where $v_a(t)$ is either the x or z component of the electron velocity for the nondipole and dipole harmonic intensities $S_x(\Omega)$ and $S_z(\Omega)$, respectively. In the velocity form for the harmonic intensity which we use here, we do not need to introduce additional powers of harmonic frequency, which would be present had we used length or acceleration forms [45]. The factor $W(t)$ in Eq. (20) is the window function [46], for which we employ the Hann form: $W(t) = \sin^2(\frac{\pi t}{T_1})$.

The most noticeable effects that the relativistic nondipole corrections produce are the appearance of harmonic photons polarized in the laser propagation direction [24–26] and the appearance of even-order harmonics in the HHG spectra [31,47]. The LOPT picture allows to explain these features transparently. Substituting the expression of Eq. (16) for the LOPT wave function into the matrix element,

$$\langle\Psi^{\rm LOPT}(t)|\hat{\boldsymbol{v}}|\Psi^{\rm LOPT}(t)\rangle \approx \hat{\boldsymbol{x}}v_x(t) + \hat{\boldsymbol{y}}v_y(t) + \hat{\boldsymbol{z}}v_z(t), \tag{21}$$

defining the leading-order contributions to the expectation value of electron velocity, one obtains

$$v_z(t) = \langle\Psi_{\rm d}(t)|\hat{v}_z|\Psi_{\rm d}(t)\rangle. \tag{22}$$

For the geometry we use, the evolution operator $\hat{U}_{\rm d}(t,\tau)$ commutes with $\hat{l}_z$ the z components of the angular momentum; i.e., it is a conserved quantity for the quantum evolution driven by the dipole Hamiltonians (13) and (14). $\hat{l}_z$, therefore, has a definite value $l_z = 0$ in the state described by the wave function $\Psi_{\rm d}(t)$, and the matrix element $\langle\Psi_{\rm d}(t)|\hat{v}_x|\Psi_{\rm d}(t)\rangle$ vanishes because of the well-known dipole selection rules [42]. The leading-order contribution to $v_x(t)$ is, therefore, of the order of c^{-1}, and is given by the expression

$$\begin{aligned} v_x(t) &= \langle\Psi_{\rm d}(t)|\hat{v}_x|\Psi^{(1)}_{\rm nd}(t)\rangle + \langle\Psi^{(1)}_{\rm nd}(t)|\hat{v}_x|\Psi_{\rm d}(t)\rangle \\ &= 2{\rm Re}\langle\Psi_{\rm d}(t)|\hat{v}_x|\Psi^{(1)}_{\rm nd}(t)\rangle \\ &= 2{\rm Im}\left(\int_0^t \langle\Psi_{\rm d}(t)|\hat{p}_x\hat{U}_{\rm d}(t,\tau)\hat{H}_{\rm nd}(\tau)|\Psi_{\rm d}(\tau)\rangle\,d\tau\right). \end{aligned} \tag{23}$$

In the last line of Eq. (23) we used expression (17) for $\Psi^{(1)}_{\rm nd}(t)$. The same dipole selection rules [42] and the structure of Eq. (17) ensure that the contribution of the order of c^{-1} to $v_y(t)$ is zero. The leading-order contribution of the nondipole effects is, therefore, nonzero only for the x component of the electron velocity. The orientation of the dipole velocity due to this relativistic contribution results, thus, in the appearance of the harmonic photons polarized in the propagation direction in accordance with the observations made in Refs. [24–26].

As we mentioned above, the appearance of the even-order harmonics can be understood as a result of violation of the symmetry of the electron trajectories responsible for the emission of harmonic photons in the dipole approximation [27]. From the LOPT perspective this effect can be explained as follows. As one can see from Eqs. (14) and (15), the dipole interaction operator (14) has odd parity, i.e., it couples states of different parities, while the nondipole operator (15) has even parity. Employing a somewhat lousy language, we might say that the presence of these two atom-field interaction Hamiltonians can be described as the presence of two kinds of photons: the "dipole" photons and the "nondipole" photons, whose emission and absorption are governed by the operators (14) and (15), respectively. Using these notions and the LOPT expression for $v_x(t)$ in Eq. (23), the contribution of the nondipole interaction to the formation of the Nth-order harmonic can be described as absorption of $N-1$ "dipole" photons and one "nondipole" photon, with subsequent recombination to the atomic ground state accompanied by emission of a harmonic photon with frequency $N\omega$. Using the informal terminology which we adopted, one might say that the emitted harmonic photon is of the "dipole" nature since spontaneous emission satisfies the dipole selection rules. Conservation of the total parity for the combined system of atom and the "dipole" and the "nondipole" photons implies then that N must necessarily be even.

Besides providing a simple physical picture of the appearance of even-order harmonics, the LOPT approach which we described above can be used as a test of the accuracy of our solution to the TDDE. To do such a test we performed calculations of the expectation values of electron velocity using TDDE and LOPT approaches for the cosine-pulse form shown in Fig. 1, with the vector potential in Eq. (5) given by the equation $\boldsymbol{A}(x,t) = -\boldsymbol{e}_z\frac{E_0}{\omega}\sin^2(\frac{\pi u}{T_1})\sin\omega u$, where $\omega = 0.057$ a.u., $E_0 = 0.0534$ a.u., and $u = t - x/c$. A comparison of the TDDE results obtained using Eq. (19) and the LOPT results

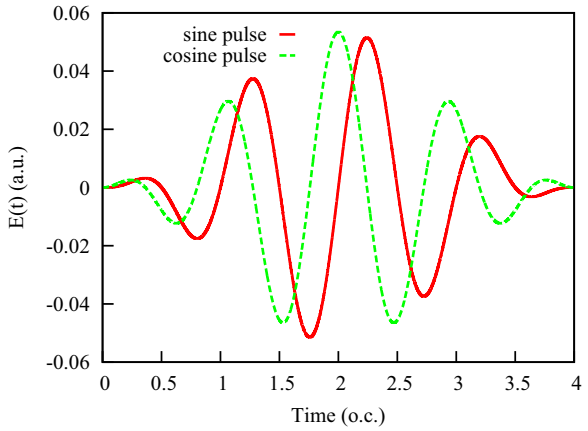

FIG. 1. Pulse shapes $E(t)$ employed in the calculations.

obtained using Eq. (23) for the x component of electron velocity is shown in Fig. 2. The results of the LOPT treatment prove to be virtually identical to the results of the TDDE calculation, which is not surprising given that the relativistic corrections could be expected to be small for the field parameters we consider.

III. RESULTS

We report below results which we obtained from our TDDE calculations for dipole $S_z(\Omega)$ and nondipole $S_x(\Omega)$ harmonic intensities for different targets. HHG spectra were obtained by computing electron velocity as prescribed by Eq. (19) and using Eq. (20) to compute harmonic intensities. Calculations were performed using the sine waveform shown in Fig. 1 with the electric field given by the equation $E(u) = E_0 \sin^2 \frac{(\pi u}{T_1)} \sin \omega u$. We report below results for the base frequencies $\omega = 0.114$ a.u. (wavelength of 400 nm) and $\omega = 0.057$ a.u. (wavelength of 800 nm). In Fig. 3 we show HHG spectra that we obtained for the driving pulse wavelength $\lambda = 400$ nm and different field strengths for various targets. Figure 3 shows both dipole $S_z(\Omega)$ and nondipole $S_x(\Omega)$

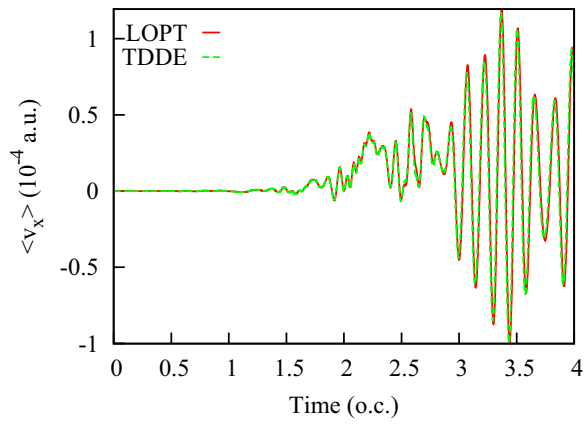

FIG. 2. Expectation value of the x component of the electron velocity as a function of time obtained in TDDE and LOPT calculations. Cosine pulse with $E_0 = 0.0534$ a.u., $\omega = 0.057$ a.u., has been used in the calculation.

harmonic intensities. The vertical lines in the figures show positions of the classical cutoffs given by the well-known $3.17U_p + I_p$ (here $U_p = E_0^2/4\omega^2$ and I_p are ponderomotive and ionization energies, respectively) rule of the three-step model [27,28]. In Fig. 4 we zoom in on the parts of the harmonic spectra more closely to demonstrate the presence of odd- and even-order harmonics in the dipole and nondipole spectra, respectively. Quite expectedly, the behavior of the dipole intensity $S_z(\Omega)$ shown in Fig. 3 agrees very well with the three-step model predictions, exhibiting a sharp drop in magnitude after reaching the classical cutoff. The nondipole $S_x(\Omega)$ spectra mimic this behavior very closely. This may be not surprising if we make use again of the LOPT picture of formation of the nondipole harmonics we presented above, which relied on the notions of "dipole" and "nondipole" photons with operators describing their interactions with an atom given by Eqs. (14) and (15), respectively. We remind that in the framework of this picture the Nth nondipole harmonic is produced as a result of the absorption of $N-1$ "dipole" photons and one "nondipole" photon. As far as the harmonic spectra are concerned, the mechanism responsible for the formation of the nondipole harmonic emission differs thus from the mechanism of the emission of the dipole harmonics only in the replacement of one "dipole" photon with a "nondipole" one. This replacement leads to the replacement of the odd-order harmonics in the spectra by the even-order ones and results in an overall drop in magnitude in the harmonic spectra due to the presence of the additional factor of c^{-1} in the nondipole interaction operator (15).

The energy and parity conservation considerations which lead us to the general conclusions about the character of the nondipole spectra do not tell us anything about temporal dynamics of the formation of the nondipole harmonics. We can have a glimpse of this temporal dynamics by analyzing Gabor transforms [48] of dipole and nondipole velocities:

$$T_a(\Omega, t) = \int_0^{T_1} v_a(\tau)\Phi^*(t, \tau, \Omega)d\tau, \tag{24}$$

where $\Phi(t, \tau, \Omega) = \exp\{i\Omega\tau - (t-\tau)^2/2(x_0T)^2\}$, the parameter x_0 determines resolution in the temporal domain, and T is an optical cycle of the laser field. The Gabor transform, as well as the closely related wavelet transform, allows us to take a look simultaneously at both time and frequency domains, and allows to determine, in particular, when different harmonics are emitted [49–51]. We used $x_0 = 0.1$ in the calculations below. This value of x_0 gives us rather poor resolution in the frequency domain, but high resolution in the time domain, which is of interest to us presently.

The absolute values $|T_a(\Omega, t)|$ for both dipole and nondipole velocities are shown in Figs. 5 and 6 for the SR Yukawa and hydrogen atoms. One can see that, dynamically, the formation of dipole and nondipole harmonics proceeds quite differently. For both Yukawa and hydrogen atoms, systems emission of the nondipole harmonics is strongly suppressed at the early stages of pulse development, and emission times for the nondipole harmonics are shifted with respect to the dipole radiation bursts. Such behavior could be anticipated by looking at Fig. 2 which shows that the x component of the velocity starts actually to respond to the field only for times

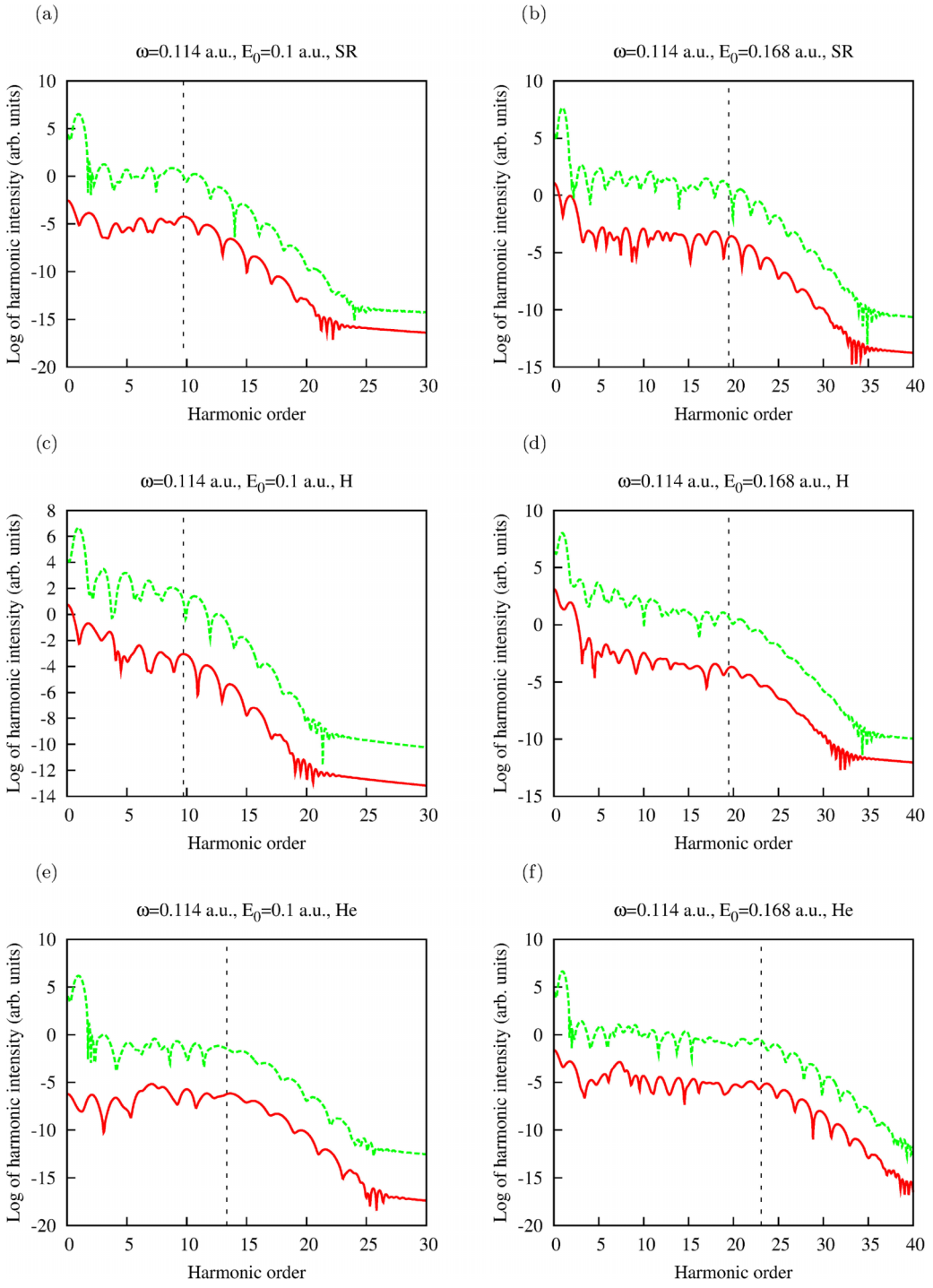

FIG. 3. Dipole (dashed green) and nondipole (red solid) harmonic intensities for the pulse wavelength $\lambda = 400$ nm for the SR Yukawa, hydrogen, and He atoms. Vertical dashed lines show cutoff positions.

approaching the midpoint of the pulse. The reason for this could be traced back to the character of the fully quantum expression for the velocity component v_x in the second LOPT equation (23), with time integration on the right-hand side of this equation smoothing out high-frequency oscillations. To elucidate this issue further we performed a simple classical calculation of the emitted photon energy as a function of the recombination time using the physical picture provided by the three-step model. We assume that the electron is ionized at the moment of time $t_{\rm ion}$ and returns to the parent ion at the moment of time $t_{\rm ret}$, emitting a harmonic photon with energy $E_{\rm ret} + I_p$. As is usually assumed in the three-step model calculations, we consider only the effect of the external field (5) on the electron motion, neglecting completely the ionic potential. The only difference between our calculation and the traditional three-step model analysis of the harmonic emission

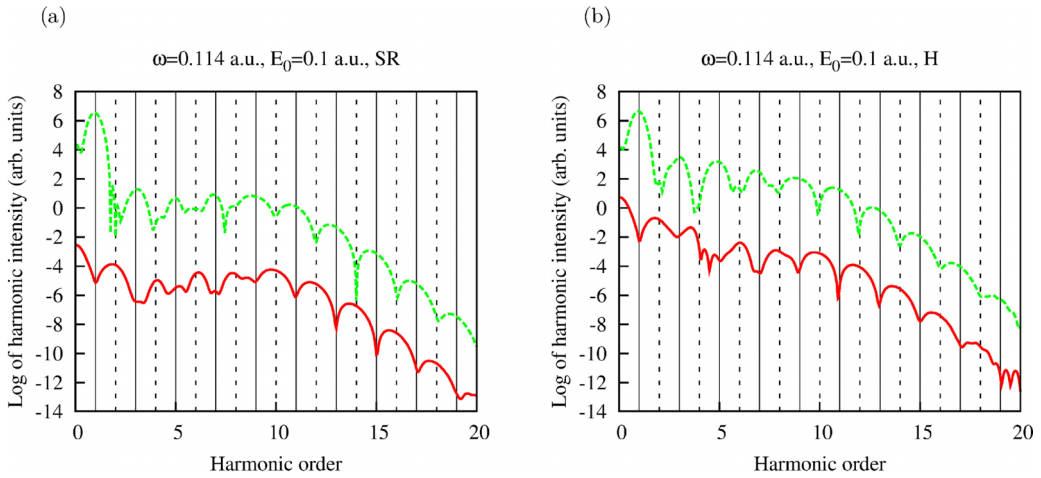

FIG. 4. Dipole (dashed green) and nondipole (red solid) harmonic intensities for the pulse wavelength $\lambda = 400$ nm for harmonics with orders $n \leqslant 20$ for the SR Yukawa and hydrogen atoms. Vertical solid and dashed lines show positions of odd- and even-order harmonics, respectively.

is that we take into account effect of the Lorentz force due to the magnetic field of the pulse. We simulate electron motion in a plane [which is the (x, z) plane for the geometry we employ], solving the set of the classical Newton equations, which for the fields configuration, geometry, and atomic units system we employ, can be written as

$$\ddot{x} = -\frac{v_z}{c}E(t),$$
$$\ddot{z} = -E(t) + \frac{v_x}{c}E(t). \tag{25}$$

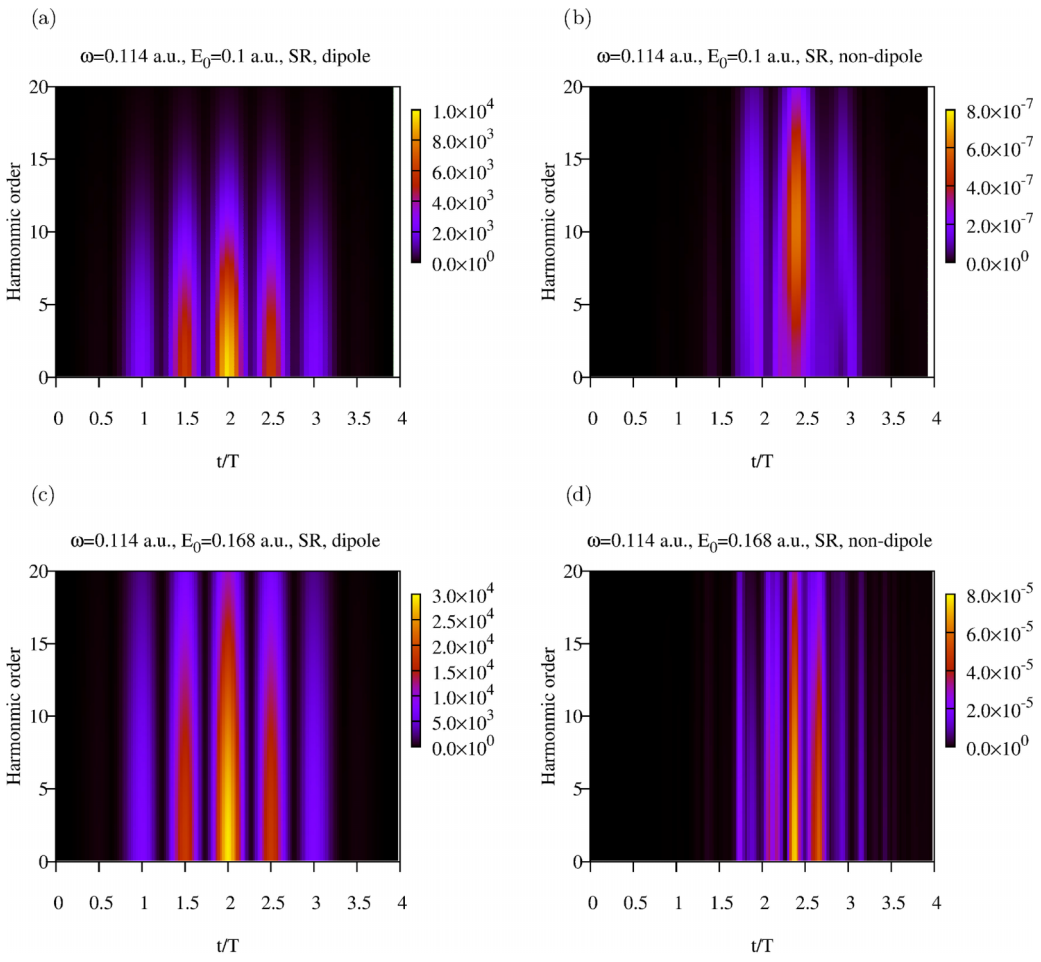

FIG. 5. Gabor transform $|T(\Omega, t)|$ for the pulse wavelength $\lambda = 400$ nm and different field strengths for the SR Yukawa atom.

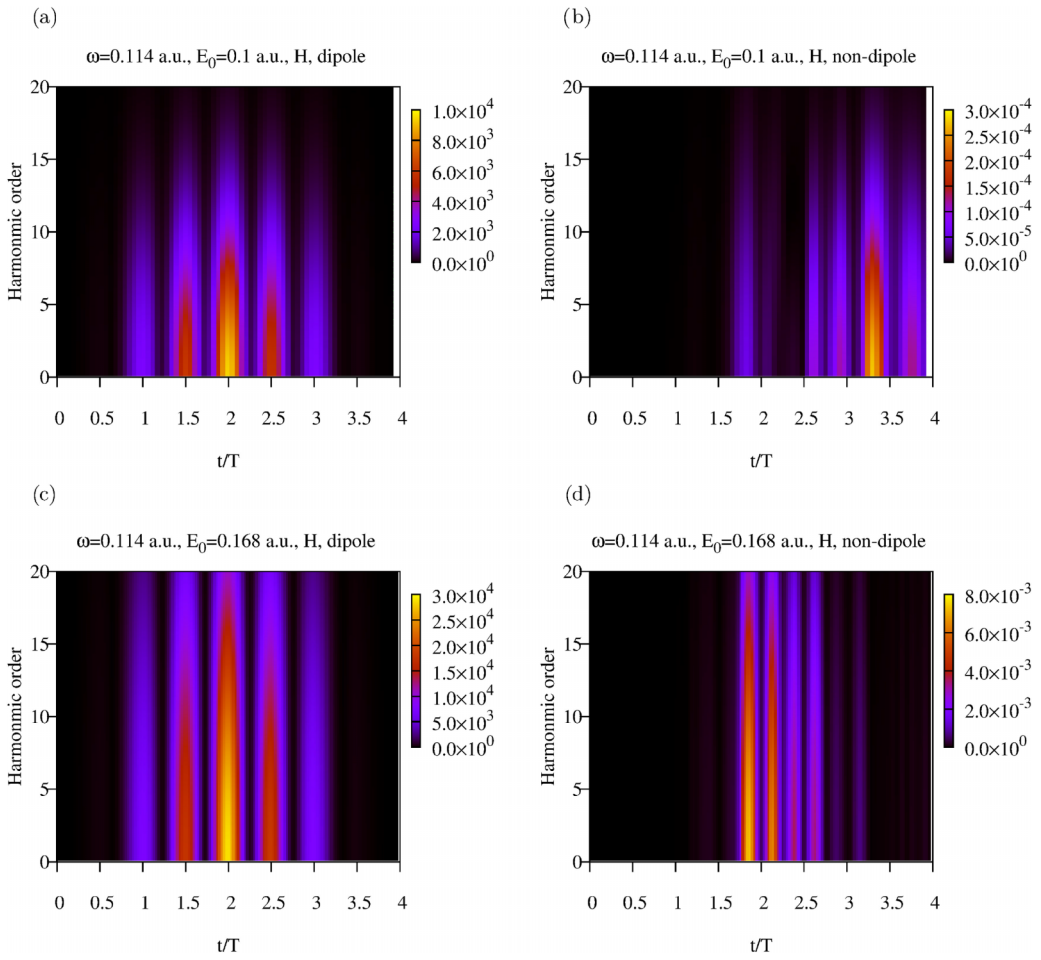

FIG. 6. Gabor transform $|T(\Omega, t)|$ for the pulse wavelength $\lambda = 400$ nm and different field strengths for the hydrogen atom.

Following the prescription of the traditional three-step model we solve Eqs. (25) with zero initial conditions imposed at the ionization time: $v_x(t_{\rm ion}) = v_z(t_{\rm ion}) = 0$ and $x(t_{\rm ion}) = z(t_{\rm ion}) = 0$. We assume that the electron trajectory returns to the origin if, at the moment of time $t_{\rm ret}$, the z coordinate of the electron trajectory changes sign.

Figure 7(a) shows results of such a simulation, which qualitatively agree with the dynamics of the dipole harmonics emission shown in Figs. 5 and 6, with bursts of harmonics emission occurring every half cycle of the laser pulse. To be able to apply this classical analysis to the emission of the nondipole harmonics we must, however, introduce one essentially quantum ingredient in the model described by the classical equations (25). Emission of the nondipole radiation differs from the emission of the dipole harmonics in one important aspect. For the geometry we employ, the dipole harmonics photon emission process satisfies the selection rule $\Delta M = 0$, where M is the z projection of the electron angular momentum. On the other hand, emission of the nondipole harmonic photon, as can be seen from the LOPT analysis we presented above, must satisfy the selection rule $\Delta M = \pm 1$. This means that for the ground s state that we consider, nondipole radiation can be emitted only by electrons with nonzero angular momentum. We can incorporate this fact in our classical model by introducing a filter parameter f in the simulations, and considering only those returning trajectories for which at the moment of time $t_{\rm ret}$ the squared classical angular momentum value exceeds the threshold value set by the filter parameter f. Results of such calculations are shown in Figs. 7(b)–7(d) for different values of the filter parameter f. One can see that by increasing the value of the filter parameter, we make the classical picture in Fig. 7 look more like the Gabor transform results shown in Figs. 5 and 6. In particular, Figs. 7(c) and 7(d) show the absence of the nondipole harmonics emission during the first two cycles of the laser pulse, the feature which is also demonstrated by the quantum analysis based on the Gabor transform in Figs. 5 and 6. Applying a nonzero filter parameter does not change, however, the maximum energy $E_{\rm ret}$ of the returning electron, which explains why nondipole harmonic emission spectra exhibit essentially the same cutoffs as the dipole harmonic emission spectra. This simple classical picture of the formation of the nondipole harmonics, which takes as a quantum ingredient only the requirement that the electron angular momentum on the returning trajectories should exceed a certain threshold value, agrees, thus, qualitatively with the fully quantum picture. We also performed TDDE calculations for the pulse base frequency $\omega = 0.057$ a.u. (corresponding to the wavelength of 800 nm). In Figs. 8 and 9 we show harmonic spectra we obtain from TDDE for the SR Yukawa and hydrogen atoms. Figure 10 shows results of the analysis of the temporal dynamics of the harmonic formation based on

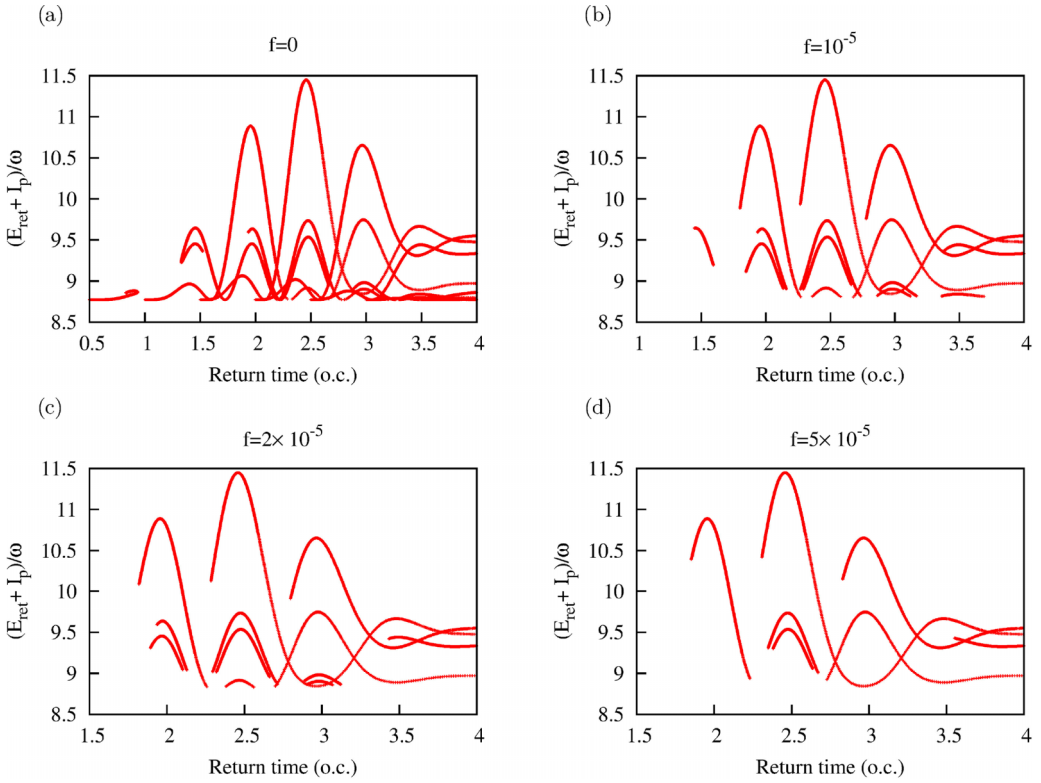

FIG. 7. Classical calculations of emitted photon energy as a function of return time for the (a) dipole harmonic radiation and [(b)–(d)] nondipole harmonic radiation with different filter parameters.

the Gabor transform (24). These figures show essentially the same picture as the results we presented above for the driving pulse wavelength of 400 nm. The spectra of the nondipole harmonics follow closely the classical dipole cutoff rule, and differ in this respect from the dipole emission spectra only in their intensity. Temporal pictures of the harmonics formation in the dipole and the nondipole cases are, however, totally different. The main difference is, just as in the case of the driving pulse wavelength of 400 nm, the absence of the harmonic emission at the early stages of the pulse development, the feature which we explained above using the results of the classical calculations shown in Figs. 7(c) and 7(d). The factor which is responsible for the difference in intensity between the dipole and nondipole harmonics is the additional factor of c^{-1} which, as one can see from Eqs. (23) and (15), is present in the LOPT formula for the x component of the velocity. The presence of this factor in v_x leads to a dampening factor of c^{-2} in the expression for the nondipole harmonics intensity. It is rather difficult to obtain a more detailed insight about the relative magnitude of the dipole and nondipole harmonic intensities from the cumbersome LOPT expressions, Eqs. (22) and (23). One can, however, obtain a simple estimate using the reasoning based not on the Schrödinger picture that we have used so far, but on the equivalent Heisenberg picture of the

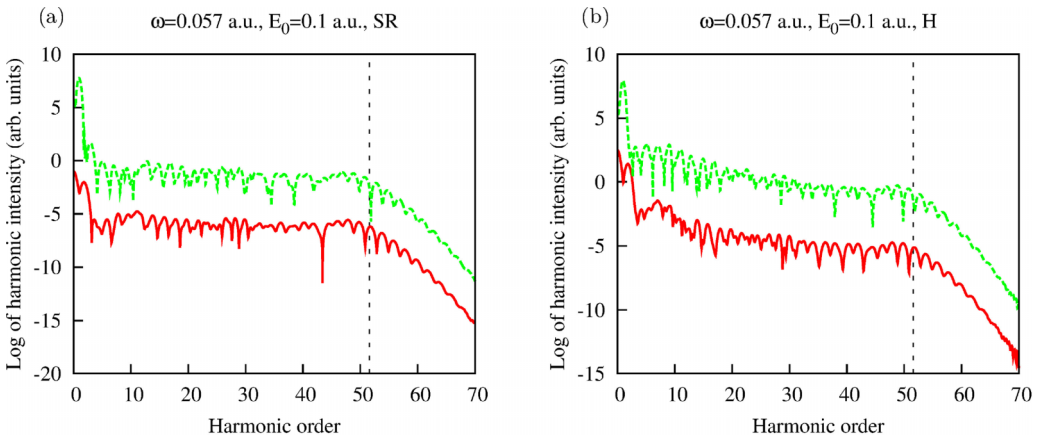

FIG. 8. Dipole (dashed green) and nondipole (red solid) harmonic intensities for the pulse wavelength $\lambda = 800$ nm for the SR Yukawa and hydrogen atoms. Vertical dashed lines show cutoff positions.

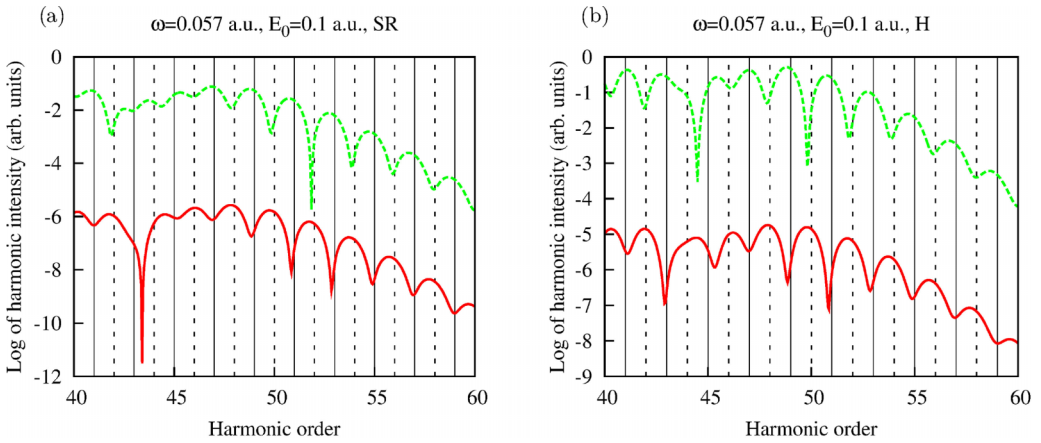

FIG. 9. Dipole (dashed green) and nondipole (red solid) harmonic intensities for the pulse wavelength $\lambda = 800$ nm for harmonics with orders $40 \leqslant n \leqslant 60$ for the SR Yukawa and hydrogen atoms. Vertical solid and dashed lines show positions of odd- and even-order harmonics, respectively.

quantum mechanics (QM). In the latter, we remind that the operators evolve in time, while the state vectors do not. We obtain, of course, the same expectation values for all physical observables in both pictures.

In the Heisenberg picture, the time evolution of the operators $\hat{\boldsymbol{r}}(t)$ and $\hat{\boldsymbol{p}}(t)$ is described by the equations [52] $i\dot{\hat{\boldsymbol{r}}} = [\hat{\boldsymbol{r}}, \hat{H}]$, $i\dot{\hat{\boldsymbol{p}}} = [\hat{\boldsymbol{p}}, \hat{H}]$, where the Hamiltonian operator in our problem is $\hat{H} = \hat{H}_{\rm atom} + \hat{H}_{\rm d}(t) + \hat{H}_{\rm nd}(t)$, with $\hat{H}_{\rm atom}$, $\hat{H}_{\rm d}(t)$, and $\hat{H}_{\rm nd}(t)$ given by Eqs. (13), (14), and (15), respectively. Calculating the commutators, one obtains the following equations of motion:

$$\begin{aligned}
\dot{\hat{x}} &= \hat{p}_x, \\
\dot{\hat{p}}_x &= -i[\hat{p}_x, \hat{V}] - \frac{\hat{v}_z}{c}E(t), \\
\dot{\hat{z}} &= \hat{p}_z + A(t) + \frac{\hat{x}}{c}E(t), \\
\dot{\hat{p}}_z &= -i[\hat{p}_z, \hat{V}],
\end{aligned} \tag{26}$$

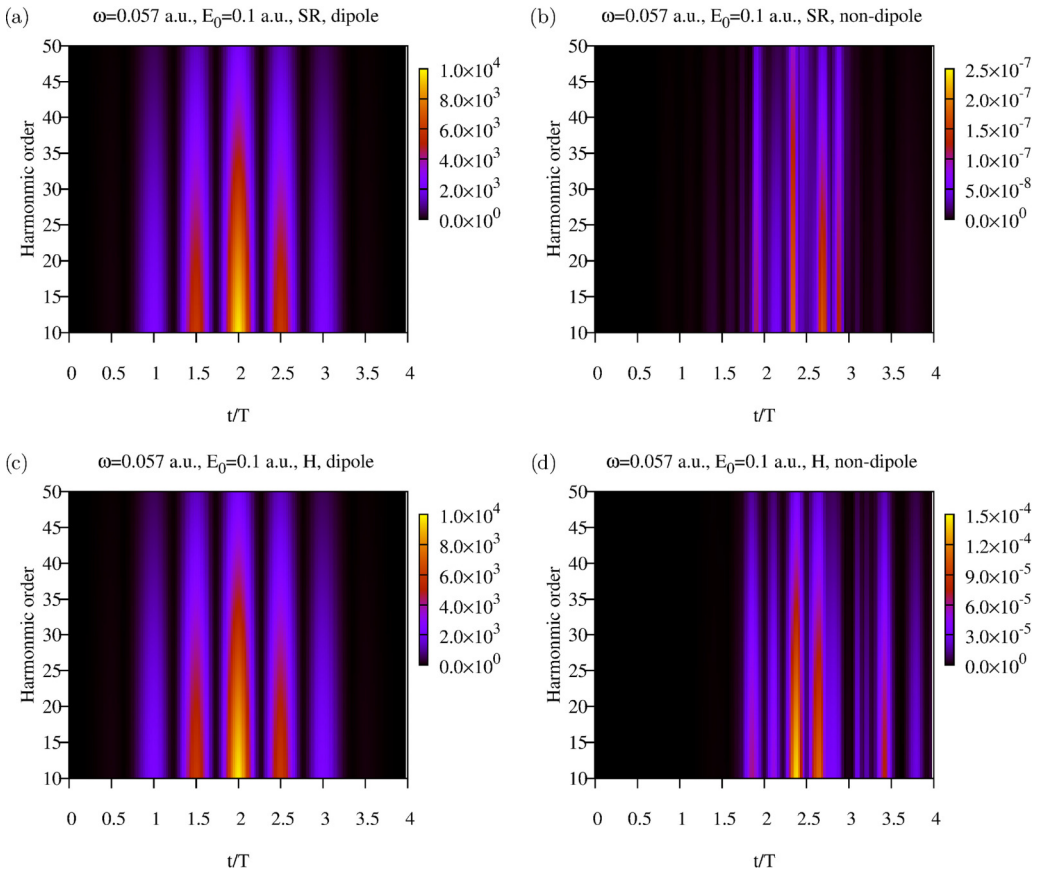

FIG. 10. Gabor transform $|T(\Omega, t)|$ for the pulse wavelength $\lambda = 800$ nm for the SR Yukawa and hydrogen atoms.

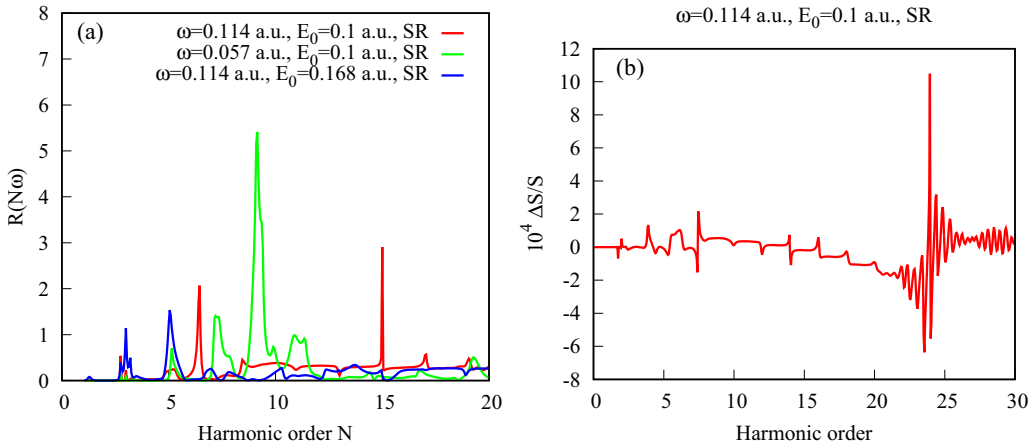

FIG. 11. (a) Estimate (31) for the ratio $R(\Omega)$. (b) Normalized difference $(S_z(\Omega) - S_z^{\rm nr}(\Omega))/S_z^{\rm nr}(\Omega)$ of the TDDE and TDSE calculations for the dipole harmonic intensities.

where $\hat{V}$ is the atomic potential operator, $\hat{v}_z = \hat{p}_z + A(t)$, and $A(t)$ and $E(t)$ are the vector potential and the electric field of the pulse. Equation (26) is the quantum-mechanical analog of the classical equations describing electron motion in the potential V in the presence of the Lorentz force. It contains the same physical information and is, therefore, equivalent to the LOPT equations (22) and (23), but it provides a more clear physical picture and can be used as a starting point for making simplifying assumptions.

From the first two of Eqs. (26) one obtains

$$\ddot{\hat{x}} = -i[\hat{p}_x, \hat{V}] - \frac{\hat{v}_z}{c}E(t). \tag{27}$$

We will make an assumption that one can omit the commutator $[\hat{p}_x, \hat{V}]$ in Eq. (27). Some justification for this operation can be provided in the case of the SR Yukawa atom, when the potential function $V(\boldsymbol{r})$ is effectively zero everywhere except for a small neighborhood of the atom. We obtain then from Eq. (27) a relation for the expectation values of the electron acceleration $a_x = \langle\phi_0|\ddot{\hat{x}}|\phi_0\rangle$ and velocity $v_z = \langle\phi_0|\hat{v}_z|\phi_0\rangle$:

$$a_x = -\frac{v_z}{c}E(t), \tag{28}$$

where $|\phi_0\rangle$ is the initial atomic state, which does not evolve in time in the Heisenberg picture. Assuming further that $E(t)$ is a monochromatic wave, $E(t) = E_0 \cos\omega t$ and calculating Fourier transforms of both sides of Eq. (28), we obtain a relation between the Fourier transforms $\tilde{v}_x(\Omega) = \int v_x(t)e^{i\Omega t}\,dt$ and $\tilde{v}_z(\Omega) = \int v_z(t)e^{i\Omega t}\,dt$:

$$-i\Omega\tilde{v}_x(\Omega) = \frac{E_0}{2c}(\tilde{v}_z(\Omega+\omega) + \tilde{v}_z(\Omega-\omega)), \tag{29}$$

from which, using the fact that for any complex numbers z_1, z_2, $|z_1 + z_2|^2 \leqslant (|z_1| + |z_2|)^2$, we obtain an inequality

$$\Omega^2 S_x(\Omega) \leqslant \frac{E_0^2}{4c^2}[\sqrt{S_z(\Omega+\omega)} + \sqrt{S_z(\Omega-\omega)}]^2. \tag{30}$$

We see from Eq. (30) that for $\Omega > \omega$ we have

$$R(\Omega) = \frac{4c^2\omega^2}{E_0^2}\frac{S_x(\Omega)}{[\sqrt{S_z(\Omega+\omega)} + \sqrt{S_z(\Omega-\omega)}]^2} \leqslant 1. \tag{31}$$

Introducing the magnitude $A_0 = E_0/\omega$ of the pulse vector potential, we can rewrite inequality (31) as

$$\frac{S_x(\Omega)}{[\sqrt{S_z(\Omega+\omega)} + \sqrt{S_z(\Omega-\omega)}]^2} \leqslant \frac{A_0^2}{4c^2}. \tag{32}$$

The ratio $R(\Omega)$ defined in Eq. (31) is shown in Fig. 11(a) for the SR Yukawa potential and various pulse parameters. Of course, we cannot expect Eq. (31) to provide a rigorous upper bound since deriving it we neglected the atomic potential in Eq. (27), which constitutes a rather drastic approximation. As one can see from Fig. 11(a), inequality (31) can indeed be violated. One can see, nevertheless, that Eq. (31), and consequently Eq. (32), provides reasonably accurate estimates of the relative magnitude of the intensities of the dipole and nondipole harmonics.

While the nonzero expectation value v_x and the appearance of the nondipole harmonics is an entirely relativistic phenomenon, the nondipole effects also modify slightly the velocity component v_z. The magnitude of this effect is of the order of c^{-2}. This can be most easily seen from the Heisenberg equations of motion (26). The equation for $v_z(t)$ [the third of Eqs. (26)] contains the term $\hat{x}E(t)/c$ on the right-hand side. Since the expectation value of x is itself of the order of c^{-1}, the resulting effect on $v_z(t)$ is of the order of c^{-2}, which will produce a relativistic correction of the order of c^{-2} for the dipole harmonic intensity. We may expect, therefore, that the normalized difference,

$$\frac{\Delta S_z(\Omega)}{S_z(\Omega)} = \frac{S_z(\Omega) - S_z^{\rm nr}(\Omega)}{S_z^{\rm nr}(\Omega)}, \tag{33}$$

where $S_z(\Omega)$ is the dipole harmonics intensity obtained in the present TDDE calculation and $S_z^{\rm nr}(\Omega)$ is the result of the nonrelativistic TDSE calculation, should be of the order of c^{-2}, i.e., we may expect $\Delta S_z(\Omega)/S_z(\Omega) \sim 10^{-4}$. That this is indeed the case can be seen from Fig. 11(b), where we show results of the TDDE and TDSE calculations performed for

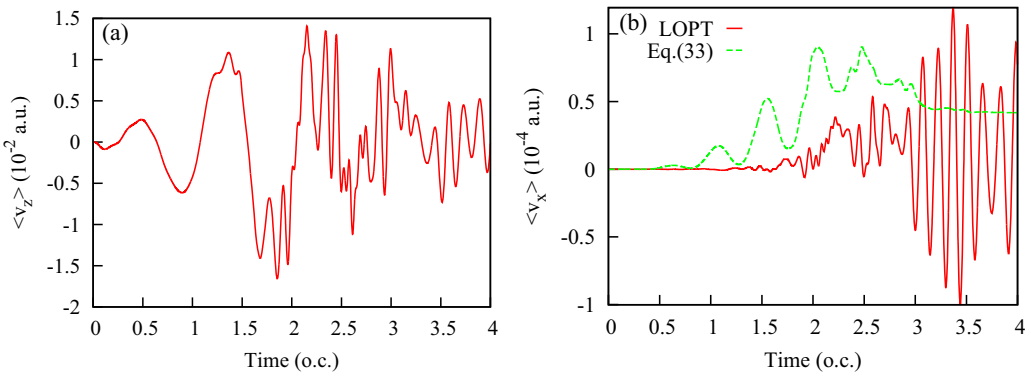

FIG. 12. (a) LOPT expectation value $v_z(t)$. (b) $v_x(t)$ obtained in the LOPT calculation and using Eq. (34). Cosine pulse with $E_0 = 0.0534$ a.u., $\omega = 0.057$ a.u. has been used in the calculations.

the same pulse parameters for the Yukawa atom. The analysis based on the Heisenberg equations of motion [Eqs. (26)] also allows to give a simple explanation for the behavior of $v_x(t)$ shown in Fig. 2, where the x component of the electron velocity starts responding to the field only for the times approaching the midpoint of the pulse. Integrating Eq. (28) we obtain for the expectation value $v_x = \langle\phi_0|\hat{v}_x|\phi_0\rangle$ (assuming that it has zero value at $t = 0$)

$$v_x(t) = -\frac{1}{c}\int_0^t v_z(\tau)E(\tau)\,d\tau. \tag{34}$$

We could have obtained the same equation by integrating the first of the set of the classical equations (25), which is not surprising given the great formal similarity between the classical mechanics and the QM in the Heisenberg picture. We show in Fig. 12(a) the expectation value $v_z(t)$ obtained in the LOPT calculation for the cosine pulse with $E_0 = 0.0534$ a.u. and $\omega = 0.057$ a.u. We show only the LOPT result. Just as in the case of $v_x(t)$, shown in Fig. 2, the TDDE and LOPT results for $v_z(t)$ differ very slightly. In Fig. 12(b) we show the LOPT expectation value $v_x(t)$, as well as the estimate for $v_x(t)$ that we obtain if we substitute the LOPT value for $v_z(\tau)$ under the integral sign in Eq. (34). One can see that the estimate thus obtained reproduces fairly well the general behavior of $v_x(t)$. In particular, it reproduces the feature that we mentioned above: the x component of the velocity begins deviating from zero appreciably only for the times approaching the midpoint of the pulse. We remind that the effect of the atomic potential on the motion in the x direction was neglected in the Heisenberg equation of motion [Eq. (28)], which we used to obtain the estimate (34). The fact that the estimate (34) reproduces qualitative behavior of the x component of electron velocity shown in Fig. 2 tells us, therefore, that this behavior might be a result of the interplay of the motion in x and z directions, which are mutually interconnected due to the presence of the Lorentz force. There is yet another factor which may result in the behavior of v_x shown in Fig. 12(b). For the field intensities that we consider, ionization occurs predominantly at the times near the main maximum t_m of the pulse field strength. Consequently, the ionized electron can gain appreciable velocity only after the peak of the field strength. Speaking more formally, this statement can be expressed by going back to the Schrödinger picture and observing that in Eq. (23) for $v_x(t)$, the norm $||\Psi_{\rm nd}^{(1)}||$ of the LOPT nondipole correction (17) differs appreciably from zero only for $t > t_m$. As a result, the integral on the right-hand side of Eq. (23) is essentially zero for $t < t_m$.

IV. CONCLUSION

We have presented results of the relativistic calculations of even-order harmonic generation from various atomic targets. Our approach was based on the numerical solution of the TDDE. The HHG spectra of the nondipole even-order harmonics were found to look qualitatively similar to the spectra of the dipole harmonics, obeying the same classical cutoff rules. The temporal formation of the nondipole harmonics, however, was found to be quite different. The results of the Gabor transform analysis show that formation of the nondipole harmonics is strongly suppressed at the beginning of the laser pulse, and bursts of the nondipole radiation are shifted in time with respect to the bursts of the dipole emission. These features are partly explained by a simple generalization of the classical three-step model, which takes into account the selection rules governing emission of harmonic photons. We modeled the effect of these selection rules by using a filter parameter, which selects the trajectories with angular momentum exceeding a certain threshold value at the recollision time.

For the field parameters we considered, the relativistic effects are still relatively weak and could be described perturbatively. LOPT provides, as we have seen, an adequate description of the nondipole effects responsible for the even-order harmonics emission. Use of the TDDE, however, is technically simpler than the calculations based on the LOPT, and opens the perspective of making an excursion into the truly relativistic domain in the future. We relied, therefore, on the TDDE-based approach in the present work. The present approach can also be generalized relatively easily to include some quantum electrodynamical (QED) effects, such as the vacuum polarization effects, or the QED strong Coulomb field radiative corrections, which can be taken into account by using effective potentials such as the Uehling potential [53] or the radiative potential proposed in Ref. [54]. The procedure we apply to solve the Dirac equation can also be used to study the process of electron-positron pair production (PP) in strong electromagnetic fields, which occurs when field strength reaches the characteristic Schwinger field strength of

1.3×10^{16} V/cm. The process of PP in both homogeneous and inhomogeneous electric fields has received considerable interest in the literature [55]. Theoretical treatment of PP in the semiclassical approximation relies on a solution of the TDDE for a given field configuration [56]. Our procedure might prove useful for this purpose, especially in the case of the spatially inhomogeneous field, which has been found to play an important role in the PP [55,57].

The numerical procedure we employ can be relatively easily generalized for the case of the many-electron relativistic Hamiltonians used in quantum chemistry calculations [58,59]. Use of the representation of the wave function analogous to expansion (6) would be, of course, impractical for systems with more than one electron if we want to use such expansions to represent the wave function in the whole space. One may use, however, the idea of the *R*-matrix approach, which separates the coordinate space in the inner region, where a suitable basis set representation can be used to represent many-electron wave functions and the outer region, where one has to concentrate on the description of a single electron motion, for which the finite difference method might be better suited. Such a strategy has been implemented with success in the framework of the so-called R-matrix incorporating time (RMT) method [60] which allows to solve the nonrelativistic TDSE for many-electron systems. One can use a similar approach in the relativistic case, relying on the results of the stationary quantum chemistry calculations [58,59] for the description of the inner region, where many-electron effects are important, and using the present procedure to solve the TDDE describing electron propagation in the outer region.

ACKNOWLEDGMENTS

This work was supported by the Institute for Basic Science (Grant No. IBS-R012-D1) and the National Research Foundation of Korea (NRF), funded by the Korean government (MIST) (Grant No. 2022R1A2C3006025). Computational works for this research were performed on the IBS Supercomputer Aleph in the IBS Research Solution Center.

[1] H. R. Reiss, Opt. Express **2**, 261 (1998).
[2] H. R. Reiss, J. Opt. Soc. Am. B **7**, 574 (1990).
[3] A. Ludwig, J. Maurer, B. W. Mayer, C. R. Phillips, L. Gallmann, and U. Keller, Phys. Rev. Lett. **113**, 243001 (2014).
[4] S. Chelkowski, A. D. Bandrauk, and P. B. Corkum, Phys. Rev. Lett. **113**, 263005 (2014).
[5] S. Chelkowski, A. D. Bandrauk, and P. B. Corkum, Phys. Rev. A **92**, 051401(R) (2015).
[6] I. A. Ivanov, J. Dubau, and K. T. Kim, Phys. Rev. A **94**, 033405 (2016).
[7] V. S. Popov, B. M. Karnakov, V. D. Mur, and S. G. Pozdnyakov, J. Exp. Theor. Phys. **102**, 760 (2006).
[8] M. Klaiber and K. Z. Hatsagortsyan, Phys. Rev. A **90**, 063416 (2014).
[9] E. Yakaboylu, M. Klaiber, and K. Z. Hatsagortsyan, Phys. Rev. A **91**, 063407 (2015).
[10] L. V. Keldysh, Sov. Phys. JETP **20**, 1307 (1965).
[11] C. T. L. Smeenk, L. Arissian, B. Zhou, A. Mysyrowicz, D. M. Villeneuve, A. Staudte, and P. B. Corkum, Phys. Rev. Lett. **106**, 193002 (2011).
[12] F. Krausz and M. Ivanov, Rev. Mod. Phys. **81**, 163 (2009).
[13] S. Chelkowski and A. D. Bandrauk, Phys. Rev. A **97**, 053401 (2018).
[14] S. Chelkowski, A. D. Bandrauk, and P. B. Corkum, Phys. Rev. A **95**, 053402 (2017).
[15] H. R. Reiss, Phys. Rev. A **87**, 033421 (2013).
[16] E. Yakaboylu, M. Klaiber, H. Bauke, K. Z. Hatsagortsyan, and C. H. Keitel, Phys. Rev. A **88**, 063421 (2013).
[17] S. Chelkowski and A. D. Bandrauk, Mol. Phys. **115**, 1971 (2017).
[18] S. V. B. Jensen, M. M. Lund, and L. B. Madsen, Phys. Rev. A **101**, 043408 (2020).
[19] D. A. Telnov and S.-I. Chu, Phys. Rev. A **102**, 063109 (2020).
[20] S. Selstø, E. Lindroth, and J. Bengtsson, Phys. Rev. A **79**, 043418 (2009).
[21] I. A. Ivanov, Phys. Rev. A **91**, 043410 (2015).
[22] I. A. Ivanov, Phys. Rev. A **96**, 013419 (2017).
[23] X. Zhu and Z. Wang, Opt. Commun. **365**, 125 (2016).
[24] R. M. Potvliege, N. J. Kylstra, and C. J. Joachain, J. Phys. B **33**, L743 (2000).
[25] N. J. Kylstra, R. M. Potvliege, and C. J. Joachain, J. Phys. B **34**, L55 (2001).
[26] C. C. Chirilă, N. J. Kylstra, R. M. Potvliege, and C. J. Joachain, Phys. Rev. A **66**, 063411 (2002).
[27] M. Lewenstein, P. Balcou, M. Y. Ivanov, A. L'Huillier, and P. B. Corkum, Phys. Rev. A **49**, 2117 (1994).
[28] P. B. Corkum, Phys. Rev. Lett. **71**, 1994 (1993).
[29] J. R. V. de Aldana and L. Roso, J. Phys. B **35**, 1633 (2002).
[30] A. D. Bandrauk and H. Z. Lu, Phys. Rev. A **73**, 013412 (2006).
[31] W. Mu-Xue, C. Si-Ge, L. Hao, and P. Liang-You, Chin. Phys. B **29**, 013302 (2020).
[32] A. Sarsa, F. J. Gálvez, and E. Buendia, J. Phys. B **36**, 4393 (2003).
[33] A. Akhiezer and V. Berestetskii, *Quantum Electrodynamics* (Wiley, New York, 1965).
[34] E. M. Lifshitz and V. B. Berestetskii, *Quantum Electrodynamics* (Pergamon Press, New York, 1982).
[35] M. Nurhuda and F. H. M. Faisal, Phys. Rev. A **60**, 3125 (1999).
[36] R. N. Hill and C. Krauthauser, Phys. Rev. Lett. **72**, 2151 (1994).
[37] P. A. M. Dirac, *The Principles of Quantum Mechanics* (McGraw-Hill, New York, 1964).
[38] I. A. Ivanov and K. T. Kim, Phys. Rev. A **92**, 053418 (2015).
[39] L. Shampine, *Numerical Solution of Ordinary Differential Equations* (Chapman & Hall, New York, 1994).
[40] A. Goldberg, H. M. Schey, and J. L. Scwartz, Am. J. Phys. **35**, 177 (1967).
[41] P. Lambropoulos and D. Petrosyan, *Fundamentals of Quantum Optics and Quantum Information* (Springer-Verlag, Berlin, 2007).

[42] I. I. Sobelman, *Introduction to the Theory of Atomic Spectra* (Pergamon Press, New York, 1972).
[43] I. A. Ivanov, Phys. Rev. A **90**, 013418 (2014).
[44] H. K. Avetissian, A. G. Markossian, and G. F. Mkrtchian, Phys. Rev. A **64**, 053404 (2001).
[45] J. C. Baggesen and L. B. Madsen, J. Phys. B **44**, 115601 (2011).
[46] R. Reiff, T. Joyce, A. Jaroń-Becker, and A. Becker, J. Phys. Commun. **4**, 065011 (2020).
[47] R. Mishra, D. Kalita, and A. Gupta, Eur. Phys. J. D **66**, 169 (2012).
[48] D. Gabor, J. Inst. Electr. Eng. **93**, 429 (1946).
[49] P. Antoine, B. Piraux, and A. Maquet, Phys. Rev. A **51**, R1750 (1995).
[50] Y. Y. Tang, L. H. Yang, J. Liu, and H. Ma, *Wavelet Theory and Its Application to Pattern Recognition* (World Scientific, Singapore, 2000).
[51] B. Wang, T. Cheng, X. Li, P. Fu, S. Chen, and J. Liu, Phys. Rev. A **72**, 063412 (2005).
[52] L. D. Landau and E. M. Lifshitz, *Quantum Mechanics* (Pergamon Press, New York, 1977).
[53] E. A. Uehling, Phys. Rev. **48**, 55 (1935).
[54] V. V. Flambaum and J. S. M. Ginges, Phys. Rev. A **72**, 052115 (2005).
[55] H. Gies and K. Klingmüller, Phys. Rev. D **72**, 065001 (2005).
[56] G. R. Mocken, M. Ruf, C. Müller, and C. H. Keitel, Phys. Rev. A **81**, 022122 (2010).
[57] C. Kohlfürst, Phys. Rev. D **101**, 096003 (2020).
[58] H. Nakai, Bull. Chem. Soc. Jpn. **94**, 1664 (2021).
[59] W. Liu, J. Chem. Phys. **152**, 180901 (2020).
[60] M. A. Lysaght, L. R. Moore, L. A. A. Nikolopoulos, J. S. Parker, H. W. van der Hart, and K. T. Taylor, J. Phys.: Conf. Ser. **388**, 012027 (2012).